Local Thermal Conductivity Mapping of Selective Laser Melted 316L Stainless Steel

Authors: Jacob Simmons[1], Matthias Daeumer[1], Arad Azizi[1], Scott N. Schiffres[1,2]*

1 Department of Mechanical Engineering, Binghamton University, Binghamton, NY 13902.

2 Department of Materials Science & Engineering, Binghamton University, Binghamton, NY

* Corresponding author sschiffr@binghamton.edu

Keywords: Laser powder-bed fusion, additive manufacturing, thermal conductivity, thermal transport, stainless steel, 316L, metal 3d printing

Abstract

The variation in thermal conductivity of 316L stainless steel samples produced with selective laser melting with a varying process parameters is investigated in the bulk and in the microscale. A critical scan rate was observed, while holding all other process parameters constant, above which the porosity started to rapidly increase. For the lowest-porosity sample, a local thermal conductivity map was produced using frequency-domain thermoreflectance. The local stainless steel thermal conductivity varied between 10.4 and 19.8 W/m-K. The average thermal conductivity of the thermal conductivity map agrees within measurement uncertainty with flash diffusivity measurements. The reduction in thermal conductivity with increasing scan rate is not fully explained by the porosity. The average measured values are less than conventionally produced bulk 316L due to the unique processing conditions of laser powder bed fusion, which modifies the crystallographic texture and microstructure.

Introduction

The properties of metal printed parts, and the variation in thermal conductivity with processing, is relatively unexplored. We investigate the thermal conductivity of selective laser melted 316L stainless steel. With additive manufacturing of metal components becoming increasingly common, understanding the properties of selective laser melted parts is increasingly important, and the thermal conductivity is important to many heat transfer related applications.

Selective laser melting (SLM) builds through laser rastering a thin metal powder to selectively melt and fuse a solid part layer-by-layer. [1] In powder bed SLM, a thin layer of metal powder, around 40µm thick, is deposited over the surface of the machine's build platform.[2] Another related method for depositing the powder is by spraying it through a nozzle onto the build area, commonly referred to as direct metal deposition.[3]

This process can currently achieve build rates of about 7cm^3/h, and continues to become more accepted by companies looking for different options when producing products.[4] A famous example of this is GE's Leap fuel nozzle. By using additive manufacturing, they were able to combine over 20 individual parts into one part and reduced the overall weight of the nozzle.[5] Another example is SpaceX additively manufacturing components of their rocket engines.[6]

Depending on the selective laser melting process parameters, the physical properties can vary significantly from the bulk properties of materials the same chemical composition material.[7] For example, Gong observed a change in ultimate tensile strength from 1237MPa to 978MPa in Ti-6Al-4V specimens produced by SLM by changing the laser power and scan rate.[7] That

translated to a 21% reduction in ultimate tensile strength. Similar analysis of thermal properties versus processing parameters are sorely lacking in the literature.

While strength of the parts produced by additive manufacturing is a common concern, the thermal properties are also important. In the previous examples, the additively manufactured parts could be subject to very high temperatures while in use. If the thermal properties of the material are not well known, there could be unexpected results from using this material in high thermal stress environments. The relationship between mechanical and thermal properties is also of interest for non-destructive testing. Furthermore, how the thermal conductivity varies in a 3D printed part locally has not been previously investigated.

The thermal properties of the SLM part are influenced by the millions of degrees per second cooling rates and highly localized melting and solidification phenomena. The quenching can lead to amorphous regions, trap impurities in the crystal, or result in smaller grains, which would all lower the thermal conductivity. There may be unfused powder that did not wet the metal below due to an oxide film and/or processing power. Porosity from voids created by pinholing and splattering also reduce the thermal conductivity.[8] There is also anisotropy induced by the melt and solidification process.[9], [10] Therefore, the thermal properties cannot be assumed to be the same as conventionally processed bulk materials.

Previous work has shown that SLM of 316L produces fine dendritic grains, on the scale of 1µm, that grow parallel to each other in separate colonies.[11]–[14] The crystallization type has also been shown to depend on the location within the melt pool.[11] Higher energy density can cause recrystallization of the underlying layer, whereas a lower energy density may not, resulting in an reduced in dendrite size.[11]

The main microstructure phase present in 316L produced from SLM is austenite, because 316L does not develop martensite when quickly cooled to room temperature.[11]–[13], [15] When cooled slowly, or not held at high temperature long enough, sigma and delta-ferrite phases, along with carbide precipitates, can develop.[15] It has been shown in previous work that as-printed SLM parts produced with 316L can contain both sigma and delta-ferrite phases in an austenite phase matrix.[14], [15] The sigma and delta-ferrite phases can be reduced or eliminated by holding the temperature of the material at temperatures above 1000°C for a certain amount of time and then quenching in water, with both the temperature and time at temperature based on the desired reduction in non-austenite phases.[15]

Different phases and precipitates found within a material can influence the thermal conductivity of the material. While studies have not been done for 316L, aluminum alloys have been studied and have shown a change in thermal conductivity with microstructure due to different heat treatments.[16], [17] However, one study concluded that Si solutes were a major factor in the changing thermal conductivity, but these shouldn't be present in 316L in large enough quantities to effect the bulk thermal conductivity.[16] While there is no literature on thermal properties of laser powder-bed fusion stainless steels, and in particular SS316L, there are several relevant thermal transport studies of bulk stainless steels, sintered stainless steels, and powdered stainless steels in literature.[18]–[24]

Methods

Six testing specimens were produced via powder bed selective laser melting using Binghamton University's EOS M290 printer and EOS's 316L stainless steel powder.[4] The laser power was set to 200W and the scan rate was varied from 750mm/s to 2000mm/s in increments of 250mm/s, with a layer height of 40um and a hatch spacing of 90um. The samples were 8x8x1.5mm to allow bulk and local thermal conductivity mapping.

The local thermal conductivities of the samples were measured by frequency domain thermoreflectance (FDTR). This process works by modulating the surface temperature by focusing a modulated laser (488 nm), referred to as the pump, onto the sample surface.[25] As the surface temperature oscillates, it causes an oscillation in the reflectance of the material at the surface. A second co-axial laser (532 nm), referred to as the probe, is then used to sample the temperature through the change in reflectance with temperature. This periodic oscillation of the reflected probe signal is sensed with a photodiode connected to a lock-in amplifier.[25]

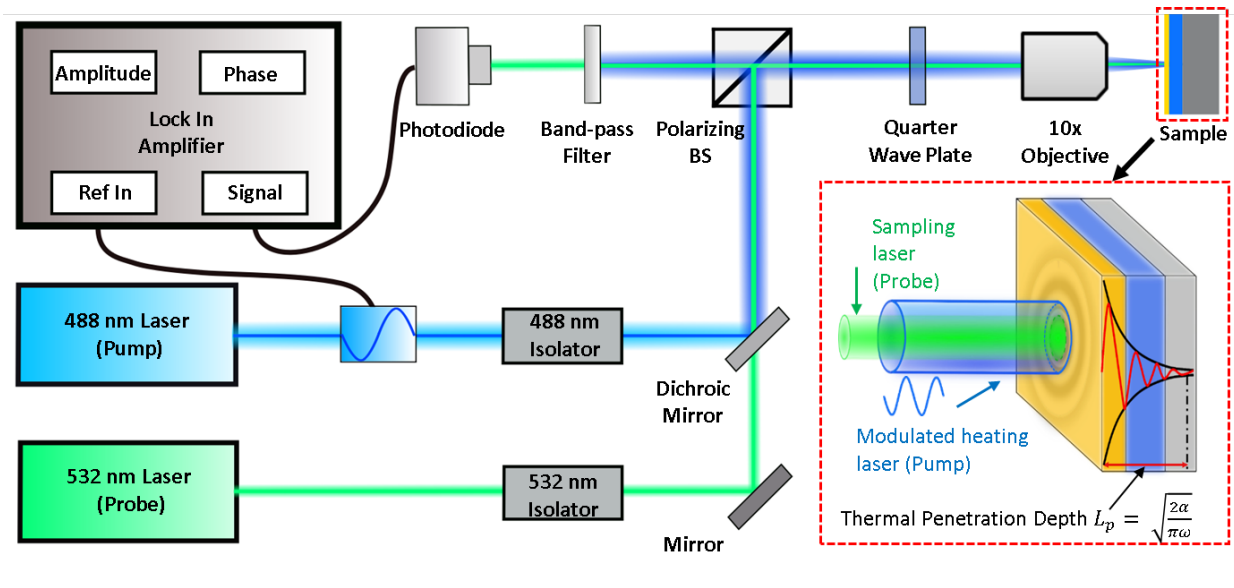

Figure 1: FDTR Experimental Setup

Based on the phase lag between the pump laser and the probe laser, the thermal properties of the material are determined.[25], [26]. An example of the phase shift versus frequency from one of the tests is shown in the following figure along with the analytical fit (Figure 2).

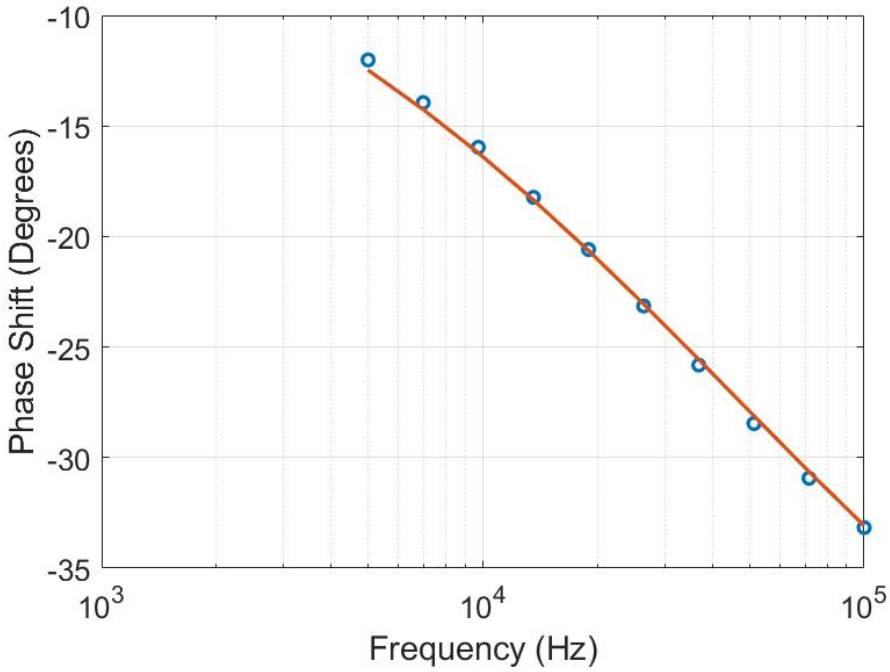

Figure 2: Representative phase shift versus frequency data for the 750mm/s sample and best analytical fit (k=14.7W/m-K)

The spatial resolution of this technique is approximately 15µm radially and in the z-direction. The spatial resolution is approximated by the following equation for thermal penetration depth.[25]

$$L = \sqrt{\frac{2\pi\alpha}{\omega}} \qquad (1)$$

In this equation, L is the thermal penetration depth, α is the thermal diffusivity and ω is the modulation frequency.[25] The testing for this sample was run over a modulation frequency of 5kHz to 100kHz, which translates into a thermal penetration depth of 65.8µm to 14.7µm respectively when using 316L as the material.

After the samples were printed, they were polished and a flash diffusivity test, which is based on the time it takes a heat pulse to travel through a material, was conducted to determine the bulk thermal conductivity of each sample.[27]–[29] The thermal diffusivities of the samples were fit via nonlinear regression fitting the experimental data from the flash diffusivity tests using MATLAB. The thermal conductivity was determined from the diffusivity by assuming literature values for the specific heat.[27] Fitting was performed using the Clark and Taylor model that accounts for radiation heat loss in the flash diffusivity experiment.[30] A comparison between this fit and the experimental data is shown in Figure 3.

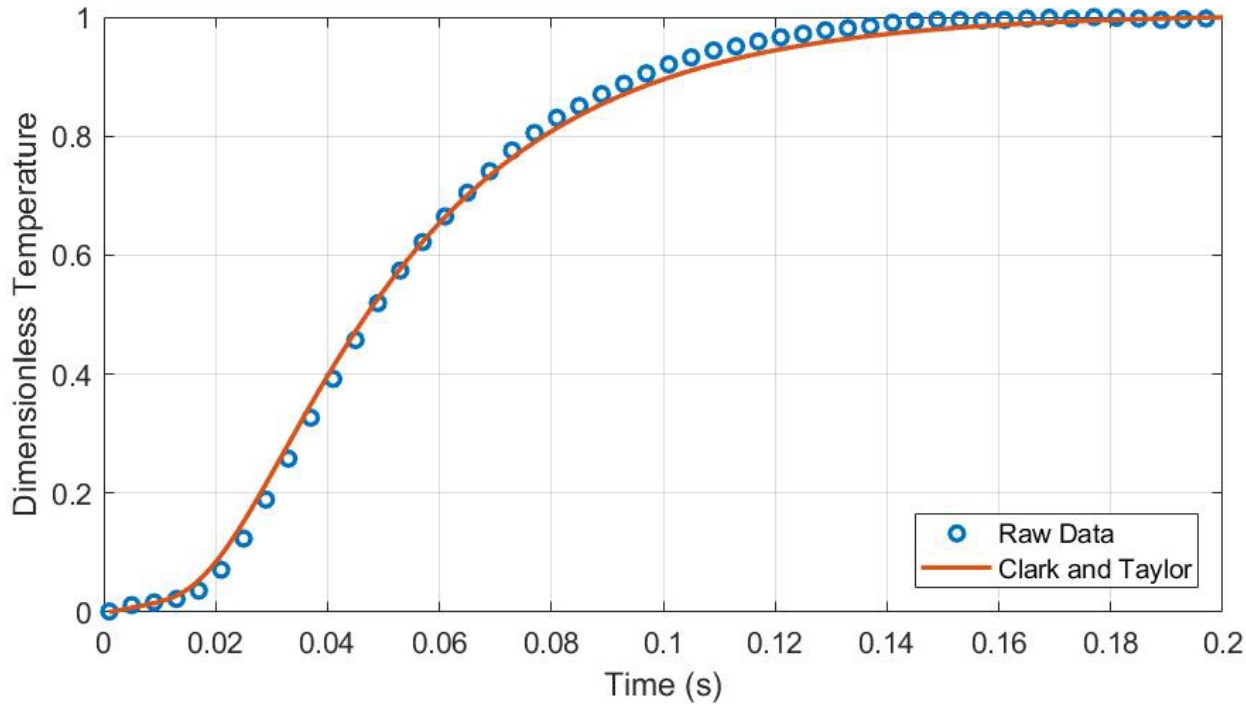

Figure 3: Representative flash diffusivity data and fit for scan rate of 750 mm/s and power 200 W (k=14.2W/m-K)

The porosity of each sample was measured optically using the ImageJ software on the images shown in Figure 4 and the results were cross-checked by measuring the mass of the samples and the volume of each sample, measured using a Quantachrome UltrapyC 1200e ultrapycnometer, to determine density.

Results

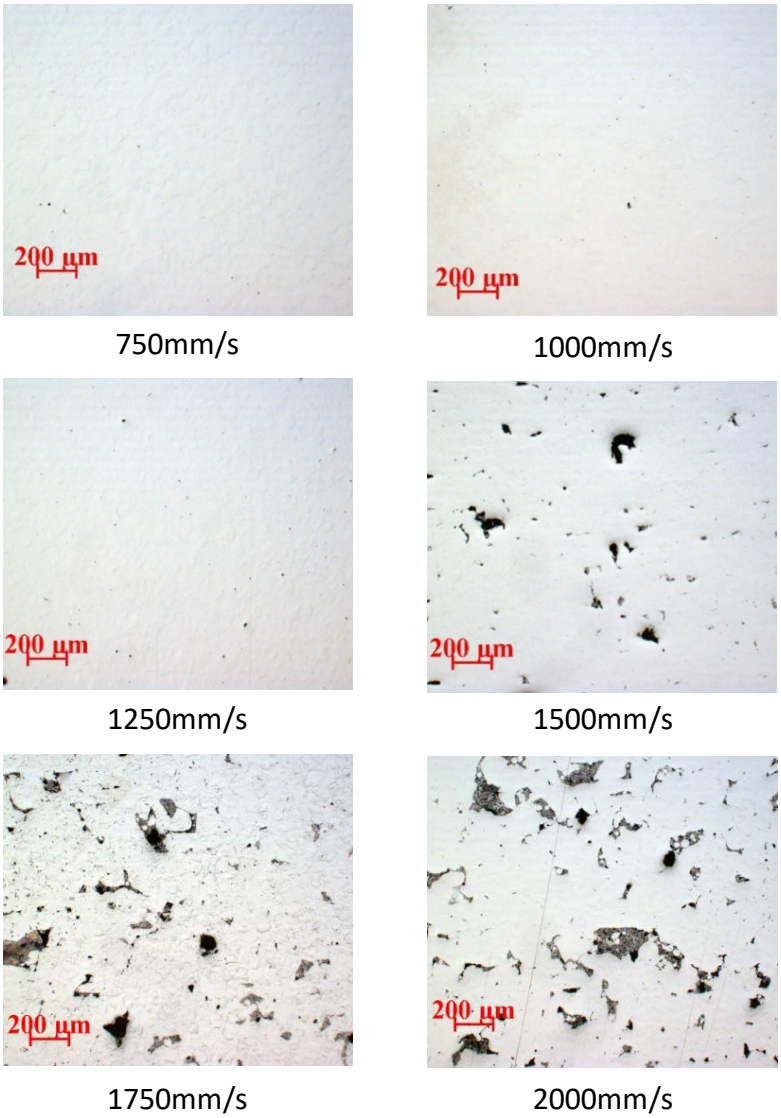

Figure 4: Polished Surface Images

The 750mm/s and 1000mm/s samples had minimal voids and the voids they did have were small, <25µm. The 1250mm/s sample had more voids, but the majority were still less than 25µm in diameter. However, the 1500mm/s sample showed a significant increase in the number and size of voids, with some voids being >100µm in diameter. Further increasing the scan rate increased the quantity of large voids, with some obtaining a diameter of over 200µm.

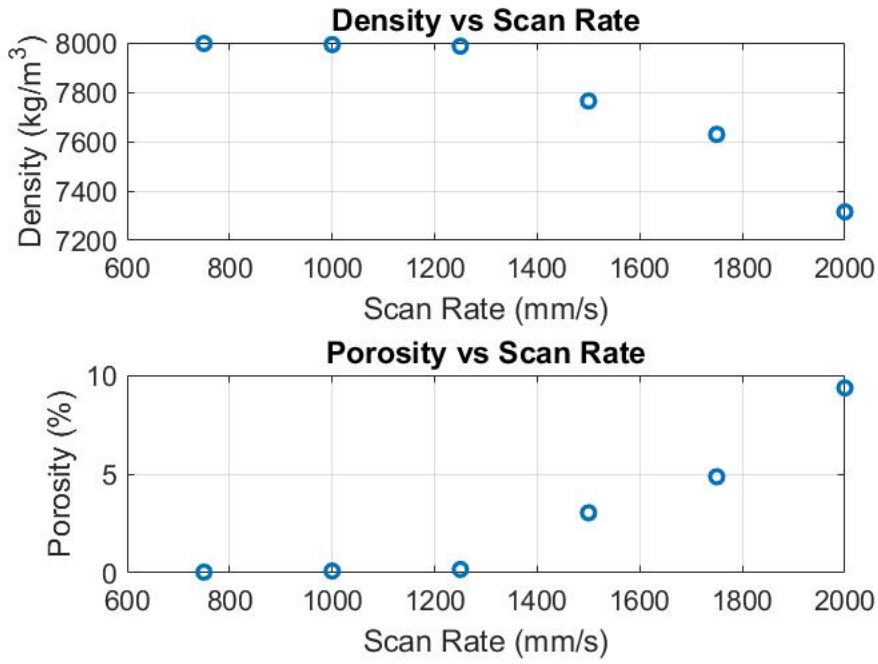

Figure 5: Density and porosity vs scan rate

At 750mm/s to 1250mm/s scan rate, the density remained relatively constant at about 7990±80kg/m^3. The highest porosity for these samples, measured optically, was 0.17%. As the scan rate was increased past 1250mm/s, up to 2000mm/s, the density started to drop and, in turn, caused the porosity to increase, up to 9.4% at 2000mm/s. The thermal conductivity of each sample was also tested using flash diffusivity and the results can be seen in Figure 6.

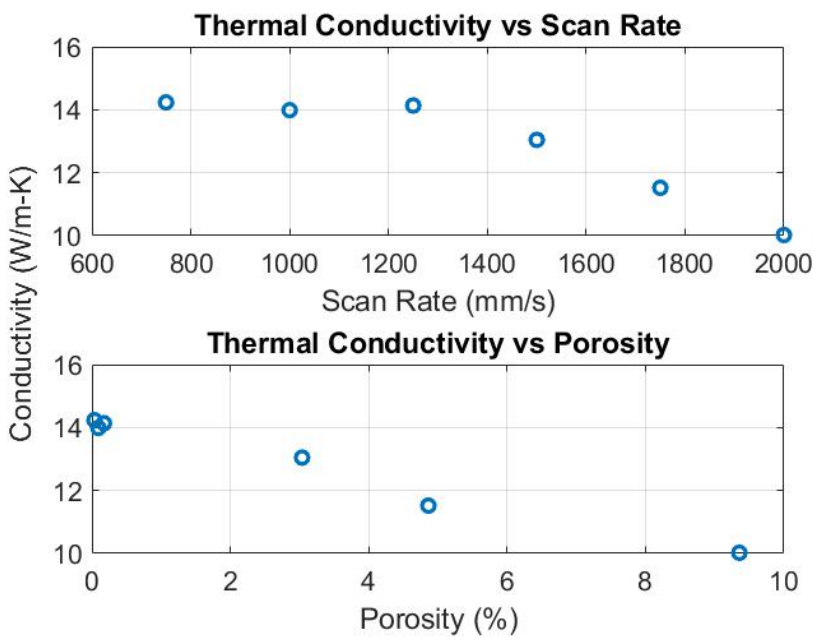

Figure 6: Thermal conductivity vs scan rate and porosity

The thermal conductivity results from the flash diffusivity experiments indicate that as the porosity increased, the thermal conductivity decreased, as expected. Heat conducting through the material would have to conduct through particles of the material in the void or convect through the gas making up the rest of the space in the void, which would significantly lower the effective thermal conductivity. The extreme case of this is shown in the results found for thermal conductivity of 316L stainless steel powder, which shows a significant reduction in the thermal conductivity of powder when compared to solid material.[22], [23]

Prior studies of traditionally sintered 304L and 316L stainless steel powders have similar trends with porosity.[19], [24] They found a relationship between porosity and thermal conductivity of 304L was well described by the empirical model of Koh and Fortinin:

$$k = k_0 \left(\frac{1 - p}{1 + 10p^2} \right) \qquad (2)$$

In this equation, k is the thermal conductivity of the sintered powder, k_0 is the thermal conductivity of the bulk material and p is the porosity of the sintered powder.[24]

The Maxwell-Garnett equation, shown in equation 3, provides analytical expression for a thermal conductivity with spherical voids.[31]

$$k_{eff} = \frac{k_m + 2k_m p \frac{k_i - k_m}{k_i + 2k_m}}{1 - p \frac{k_i - k_m}{k_i + 2k_m}} \qquad (3)$$

It does this by using the bulk conductivity of the matrix material, the volume fraction of inclusions, the porosity in this case, and the conductivity of the inclusions, assumed to be zero for this case.

Lima *et al.* also measured the properties of samples produced using traditional metal sintering of 316L. However, instead of a gradual reduction in thermal conductivity as porosity increased, like the results found for this paper, they showed a large drop in thermal conductivity at about 8% porosity.[19] These results, along with the bulk thermal conductivity results from this paper and the predicted values from Equations 2 and 3 are shown in Figure 7. It should be noted that a k_0 value of 14.6W/m-K was used in Equations 2 and 3, as this is the primary thermal conductivity of 316L at 20ºC used by other studies.[32]–[35]

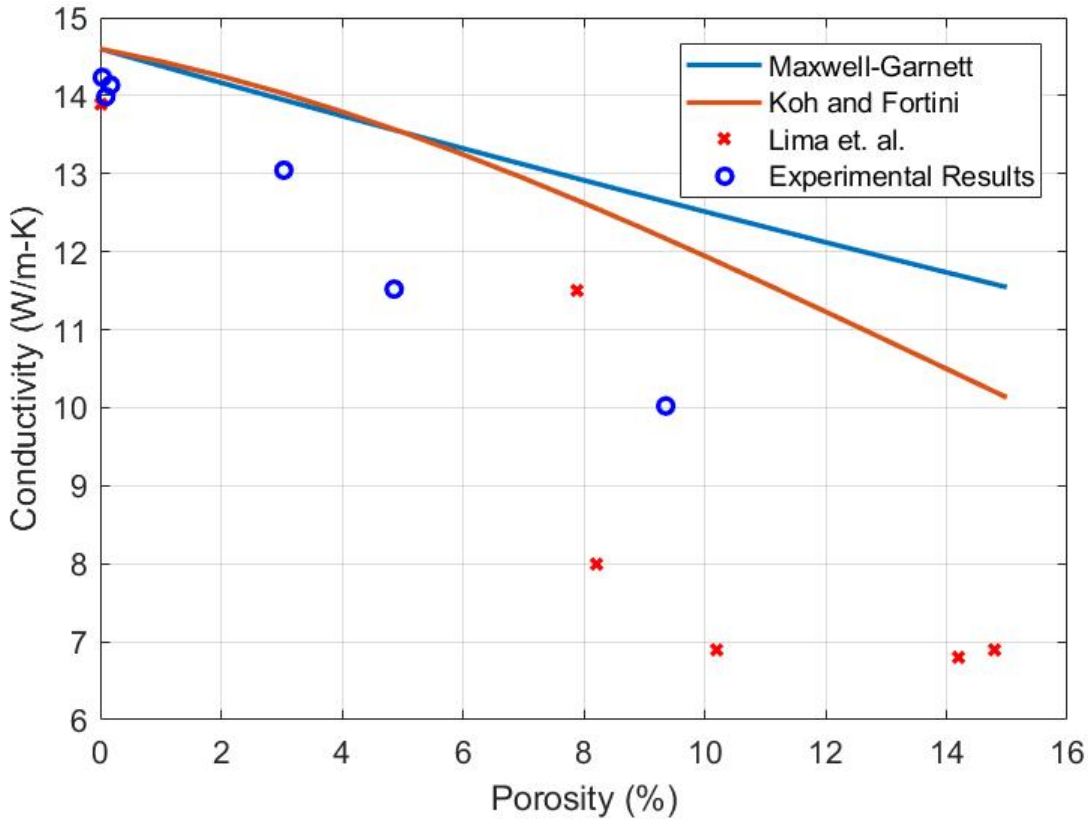

Figure 7: Experimental and Predicted Thermal Conductivity vs Porosity

Despite the shifted conductivity values at low porosity, Figure 7 shows that both the Maxwell-Garnett equation and the equation used by Koh and Fortini predict the same general trend, as was obtained for the samples tested, of a linear reduction in thermal conductivity vs porosity in the porosity range up to 10%. However, the experimental results showed a larger decrease in thermal conductivity for the same increase in porosity when compared to the results from Equations 2 and 3.

An FDTR test was also done to produce a map of thermal conductivity values on the surface of the 750mm/s scan rate sample with low porosity. A 20x20 grid of sample positions were tested with FDTR, using a spacing of 5µm between each position. The resulting thermal conductivity map is shown in Figure 8.

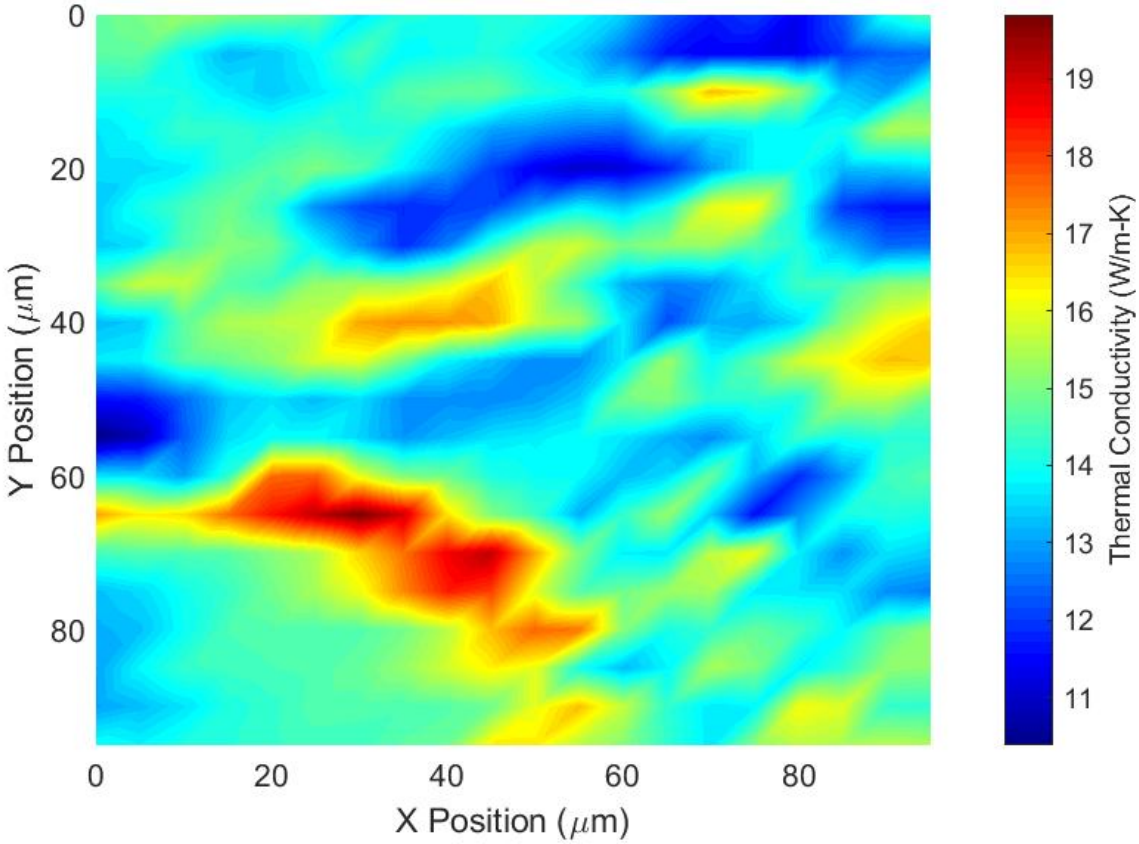

Figure 8: Thermal Conductivity Map for 750mm/s Scan Rate Sample

This map shows that the FDTR results gave a range of thermal conductivity values depending on the tested position. A histogram of the thermal conductivity values at every point was created and is shown in Figure 9. The lowest value for conductivity found in the FDTR test was 10.4W/m-K and the highest was 19.8W/m-K, with a mean of 14.3W/m-K. Many of the points had calculated thermal conductivity values in the range of 13.5W/m-K to 15.5W/m-K, which is in the expected range for the thermal conductivity of 316L previously discussed. The large variation in conductivity values over the tested area could also be due to differences in crystal grain shape and orientation, oxide and/or carbides.

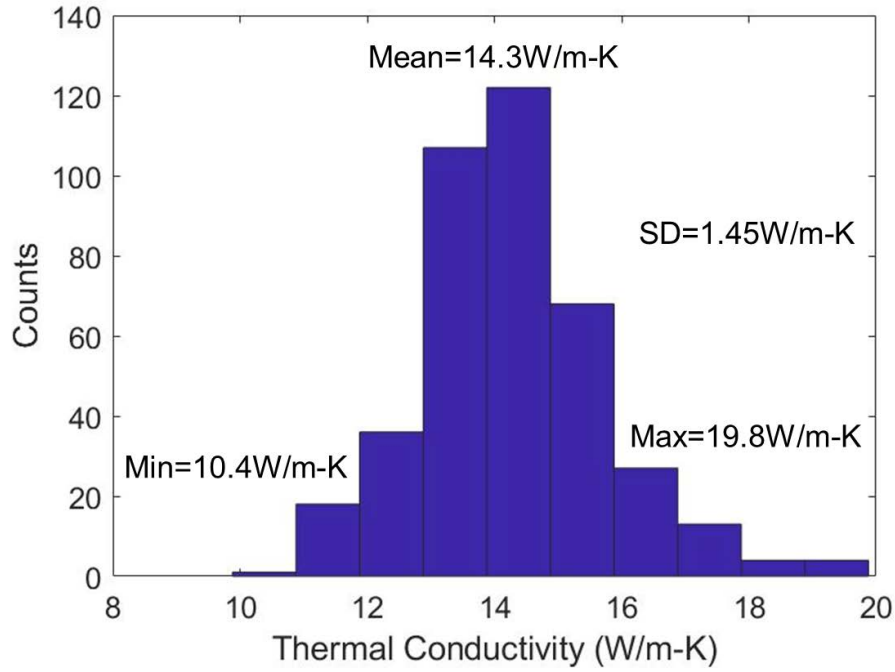

Figure 9: Histogram of FDTR Conductivity Results

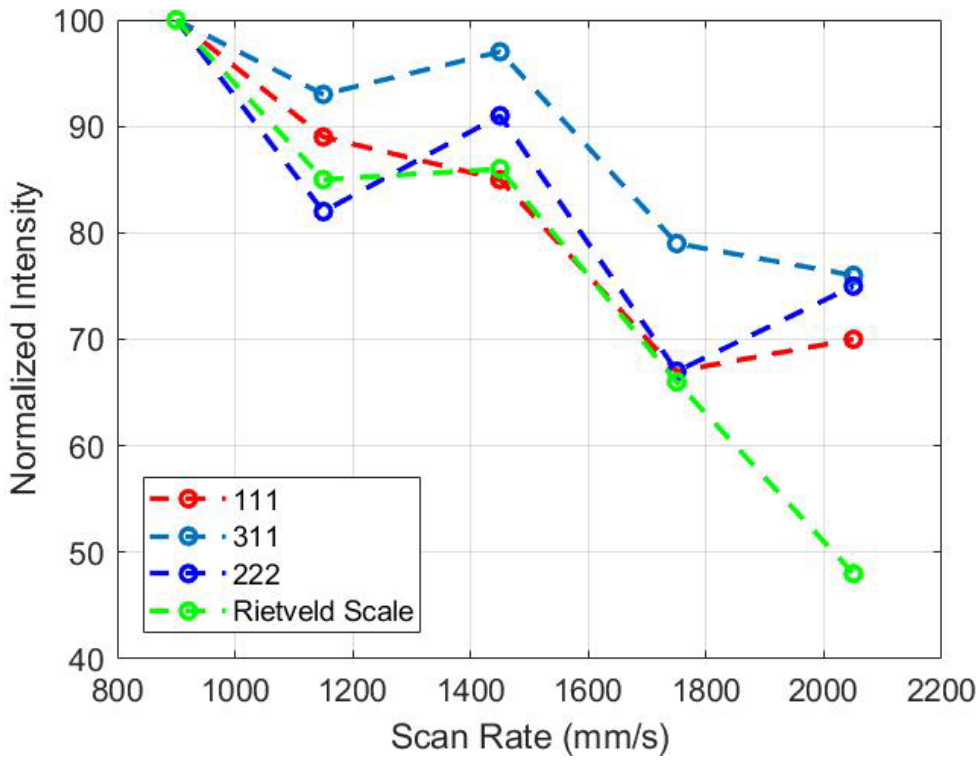

Figure 10: XRD test results

Finally, an x-ray diffraction test was performed on samples printed with the same process parameters as listed above (Figure 10). The trends in XRD intensity trend similarly to the

difference between effective medium models and experimental results. This intensity reduction may be due to amorphous or non-austenitic phases.

Conclusion

For scan rates from 750mm/s to 1250mm/s, the porosity remained less than 1% and the thermal conductivity was 14.1±0.8W/m-K. After the laser scan rate was increased past the critical value of 1250mm/s, the porosity increased rapidly to a value of 9.4% at 2000mm/s scan rate, due to incomplete fusion and the creation of voids, and the bulk thermal conductivity dropped to 10.0±0.5W/m-K. These results show that structural properties are not the only properties effected by process parameters in additively manufacturing. If the energy density of the process is too low, created by increasing the laser scan rate in this case, porosity develops and drastically reduces the thermal conductivity. These results showed a 30% reduction in thermal conductivity by simply changing the laser scan rate from 1250mm/s to 2000mm/s.

The bulk thermal conductivities are below the expected thermal conductivity *versus* porosity effective medium model by anywhere from 3-13%.[24] The unique thermal profile of SLM changes the microstructure and alters the thermal conductivity. The reduction below model predictions is an area of future research. The large variation in thermal conductivity observed in thermal conductivity mapping is likely due to variability in the crystal growth direction and crystal orientation due to the thermal gradients experienced during SLM, and is also an important area for further study.[9], [11]

Acknowledgement

We thank Dr. Peter Y. Zavalij University of Maryland, X-Ray Crystallographic Center) for his XRD help, and Scott Volk and Shawn Leonard of Incodema3D for their valuable advice. We thank Dr. Guangwen Zhou for helpful discussions. S.N.S gratefully acknowledges the support of SUNY Binghamton through his startup and the ADL's Small Grant (ADLG173). J.S. and M.D. acknowledge NSF-1742056.

References

[1] C. Y. Yap *et al.*, "Review of selective laser melting: Materials and applications," *Appl. Phys. Rev.*, vol. 2, no. 4, p. 041101, Dec. 2015.

[2] W. E. Frazier, "Metal Additive Manufacturing: A Review," *J. Mater. Eng. Perform.*, vol. 23, no. 6, pp. 1917–1928, Jun. 2014.

[3] B. Dutta, "Additive Manufacturing by Direct Metal Deposition," p. 4.

[4] "EOSStainlessSteel316L.pdf," *EOS*. [Online]. Available: https://cdn1.scrvt.com/eos/77d285f20ed6ae89/dd6850c010d3/EOSStainlessSteel316L.pdf. [Accessed: 03-Feb-2018].

[5] T. Kellner, "How 3D Printing Will Change Manufacturing," *GE Reports*, 13-Nov-2017. [Online]. Available: https://www.ge.com/reports/epiphany-disruption-ge-additive-chief-explains-3d-printing-will-upend-manufacturing/. [Accessed: 30-Jun-2018].

[6] H. Post, "SpaceX Launches 3D-Printed Part to Space, Creates Printed Engine Chamber," *SpaceX*, 31-Jul-2014. [Online]. Available: http://www.spacex.com/news/2014/07/31/spacex-launches-3d-printed-part-space-creates-printed-engine-chamber-crewed. [Accessed: 30-Jun-2018].

[7] H. Gong, "Generation and detection of defects in metallic parts fabricated by selective laser melting and electron beam melting and their effects on mechanical properties.," 2013.

[8] M. J. Matthews, G. Guss, S. A. Khairallah, A. M. Rubenchik, P. J. Depond, and W. E. King, "Denudation of metal powder layers in laser powder bed fusion processes," *Acta Mater.*, vol. 114, pp. 33–42, Aug. 2016.
[9] T. Niendorf, S. Leuders, A. Riemer, H. A. Richard, T. Tröster, and D. Schwarze, "Highly Anisotropic Steel Processed by Selective Laser Melting," *Metall. Mater. Trans. B*, vol. 44, no. 4, pp. 794–796, Aug. 2013.
[10] Y. M. Wang *et al.*, "Additively manufactured hierarchical stainless steels with high strength and ductility," *Nat. Mater.*, vol. 17, no. 1, pp. 63–71, Oct. 2017.
[11] D. Wang, C. Song, Y. Yang, and Y. Bai, "Investigation of crystal growth mechanism during selective laser melting and mechanical property characterization of 316L stainless steel parts," *Mater. Des.*, vol. 100, pp. 291–299, Jun. 2016.
[12] P. Krakhmalev, I. Yadroitsava, G. Fredriksson, and I. Yadroitsev, "Microstructure of SLM manufactured 316L and 420 grades stainless steel," *Proceeding RAPDASA 15th Annu. Int. Conf. 2014 Novemb. 6-7 Stellenbosch South Afr.*, pp. 59–66, Jan. 2014.
[13] E. Liverani, S. Toschi, L. Ceschini, and A. Fortunato, "Effect of selective laser melting (SLM) process parameters on microstructure and mechanical properties of 316L austenitic stainless steel," *J. Mater. Process. Technol.*, vol. 249, pp. 255–263, Nov. 2017.
[14] T. Kurzynowski, K. Gruber, W. Stopyra, B. Kuźnicka, and E. Chlebus, "Correlation between process parameters, microstructure and properties of 316 L stainless steel processed by selective laser melting," *Mater. Sci. Eng. A*, vol. 718, pp. 64–73, Mar. 2018.
[15] X. Chen, J. Li, X. Cheng, H. Wang, and Z. Huang, "Effect of heat treatment on microstructure, mechanical and corrosion properties of austenitic stainless steel 316L using arc additive manufacturing," *Mater. Sci. Eng. A*, vol. 715, pp. 307–314, Feb. 2018.
[16] M. Payandeh, E. Sjölander, A. E. W. Jarfors, and M. Wessén, "Influence of microstructure and heat treatment on thermal conductivity of rheocast and liquid die cast Al-6Si-2Cu-Zn alloy," *Int. J. Cast Met. Res.*, vol. 29, no. 4, pp. 202–213, Jul. 2016.
[17] J. K. Chen, H. Y. Hung, C. F. Wang, and N. K. Tang, "Effects of casting and heat treatment processes on the thermal conductivity of an Al-Si-Cu-Fe-Zn alloy," *Int. J. Heat Mass Transf.*, vol. 105, pp. 189–195, Feb. 2017.
[18] C. Y. Ho and T. K. Chu, "Electrical resistivity and thermal conductivity of nine selected AISI stainless steels," THERMOPHYSICAL AND ELECTRONIC PROPERTIES INFORMATION ANALYSIS CENTER LAFAYETTE IN, 1977.
[19] W. M. Lima *et al.*, "The effect of porosity on thermal properties: towards a threshold of particle contact in sintered stainless steel," *J. Phys. Condens. Matter*, vol. 17, no. 7, pp. 1239–1249, Feb. 2005.
[20] "Stainless Steel - Grade 316L (UNS S31603)," *AZoM.com*, 18-Feb-2004. [Online]. Available: https://www.azom.com/article.aspx?ArticleID=2382. [Accessed: 03-Jul-2018].
[21] J. C. Y. Koh and A. Fortini, "Prediction of thermal conductivity and electrical resistivity of porous metallic materials," *Int. J. Heat Mass Transf.*, vol. 16, no. 11, pp. 2013–2022, Nov. 1973.
[22] M. R. Alkahari *et al.*, "Thermal conductivity of metal powder and consolidated material fabricated via selective laser melting," in *Key Engineering Materials*, 2012, vol. 523, pp. 244–249.
[23] L. C. Wei, L. E. Ehrlich, M. J. Powell-Palm, C. Montgomery, J. Beuth, and J. A. Malen, "Thermal conductivity of metal powders for powder bed additive manufacturing," *Addit. Manuf.*, vol. 21, pp. 201–208, May 2018.

[24] J. C. Y. Koh and A. Fortini, “Thermal Conductivity and Electrical Resistivity of Porous Material.” NASA, Oct-1971.
[25] A. J. Schmidt, “Optical characterization of thermal transport from the nanoscale to the macroscale,” Massachusetts Institute of Technology, 2008.
[26] D. Cahill, “Analysis of Heat Flow in Layered Structures for Time-Domain Thermoreflectance,” *Rev. Sci. Instrum.*, vol. 75, pp. 5119–5122, Jan. 2005.
[27] “Stainless Steel - Grade 316L - Properties, Fabrication and Applications (UNS S31603),” *AZoM.com*, 18-Feb-2004. [Online]. Available: https://www.azom.com/article.aspx?ArticleID=2382. [Accessed: 18-Oct-2017].
[28] “Flash Diffusivity Method: A Survey of Capabilities,” *Electronics Cooling*, 01-May-2002. .
[29] W. J. Parker, R. J. Jenkins, C. P. Butler, and G. L. Abbott, “Flash Method of Determining Thermal Diffusivity, Heat Capacity, and Thermal Conductivity,” *J. Appl. Phys.*, vol. 32, no. 9, pp. 1679–1684, Sep. 1961.
[30] L. M. Clark III and R. E. Taylor, “Radiation loss in the flash method for thermal diffusivity,” *J. Appl. Phys.*, vol. 46, no. 2, pp. 714–719, Feb. 1975.
[31] V. A. Markel, “Introduction to the Maxwell Garnett approximation: tutorial,” *J. Opt. Soc. Am. A*, vol. 33, no. 7, p. 1244, Jul. 2016.
[32] J. C. Outeiro, D. Umbrello, and R. M’Saoubi, “Experimental and numerical modelling of the residual stresses induced in orthogonal cutting of AISI 316L steel,” *Int. J. Mach. Tools Manuf.*, vol. 46, no. 14, pp. 1786–1794, Nov. 2006.
[33] L. Bodelot, L. Sabatier, E. Charkaluk, and P. Dufrénoy, “Experimental setup for fully coupled kinematic and thermal measurements at the microstructure scale of an AISI 316L steel,” *Mater. Sci. Eng. A*, vol. 501, no. 1, pp. 52–60, Feb. 2009.
[34] J. Song, J. C. Gelin, T. Barrière, and B. Liu, “Experiments and numerical modelling of solid state sintering for 316L stainless steel components,” *J. Mater. Process. Technol.*, vol. 177, no. 1, pp. 352–355, Jul. 2006.
[35] C. Bonnet *et al.*, “Identification of a friction model—Application to the context of dry cutting of an AISI 316L austenitic stainless steel with a TiN coated carbide tool,” *Int. J. Mach. Tools Manuf.*, vol. 48, no. 11, pp. 1211–1223, Sep. 2008.